Variations of drift stability at the proposed Yucca Mountain repository

G.I.Ofoegbu
Center for Nuclear Waste Regulatory Analyses, 6220 Culebra Road, San Antonio, Texas 78238-5166
e-mail (gofoegbu@swri.edu)

ABSTRACT: Finite-element modeling of the emplacement-drift area of the potential nuclear waste repository at Yucca Mountain, Nevada, indicates significant spatial and temporal variations of drift stability resulting from spatial variation of rock-mass mechanical properties and plausible time-dependent mechanical degradation of the rock mass. Analyses were based on mechanical parameters derived through empirical correlations with rock-mass quality, Q. In the presence of stiff ground support, potential instability is higher in areas of higher Q (within the range of Q values used in the model) and is most intense at the middle of inter-drift pillars. With degraded ground support, potential instability is higher in areas of lower Q and is most intense in the roof and floor areas of the drifts. Site-specific data defining the relationships between rock-mass quality and mechanical properties are required to reduce the uncertainties associated with such calculated results.

1 INTRODUCTION

The stability of underground openings at the proposed nuclear waste repository at Yucca Mountain, Nevada, is of regulatory concern because of requirements for radiation safety and retrievability of the emplaced waste through the preclosure period. Also, the intensity and distribution of ground movements (i.e. rock deformations, collapse, and other changes that may affect the integrity or geometrical configuration of underground openings) that may occur during the postclosure period are of regulatory interest because of potential effects on waste containment. Rock fall from the roof area of emplacement drifts may cause rupture or promote corrosive damage of the waste packages. Also, rock-mass porosity and permeability and the size and shape of the emplacement drifts, all of which may be significantly modified by ground movement, are important inputs for the assessment of water seepage into the emplacement drifts. This paper presents results of thermal-mechanical analyses of the emplacement-drift area of the proposed repository, considering the effects of spatial variation of rock-mass mechanical properties and hypothesized time-dependent degradation of the rock mass and ground support.

Rock-mass mechanical properties vary both vertically and laterally at Yucca Mountain because of the layered nature of the tuffaceous rocks and variations in fracture frequency, lithophysal characteristics, and, to a lesser degree, intact-rock properties. Mechanical characterization of the rock mass has followed the traditional approach (Barton et al. 1974, Bieniawski 1979) in which intact-rock and fracture characteristics are combined using empirical rules to obtain an index value that represents the quality of the rock mass. Fracture mapping of a recently completed test drift (the Exploratory Studies Facility) enabled the development of rock-mass quality data based on the Q index of Barton et al. (1974), in an approximately north-south direction along the east boundary of the emplacement-drift area (Civilian Radioactive Waste Management System, Management and Operating Contractor 1997). The analysis model was developed to permit representation of the spatial variation of mechanical properties derived from the Q data.

2 MODEL DESCRIPTION

Analyses were performed using a two-dimensional, repository-scale, plane-strain, finite-element model of the emplacement-drift area. The model consists of an approximately north-south vertical section normal to the emplacement-drift axes (Fig.1). A total of 100 drifts were represented, with Drift #1 at the north end and Drift #100 at the south end. Drift spacing was set at 28 m center to center for a thermal-loading equivalent of 85 metric tons of uranium per acre. As a result, the model extends 3200 m horizontally (including 200-m extensions beyond the ends of Drifts #1 and #100) and 1000 m

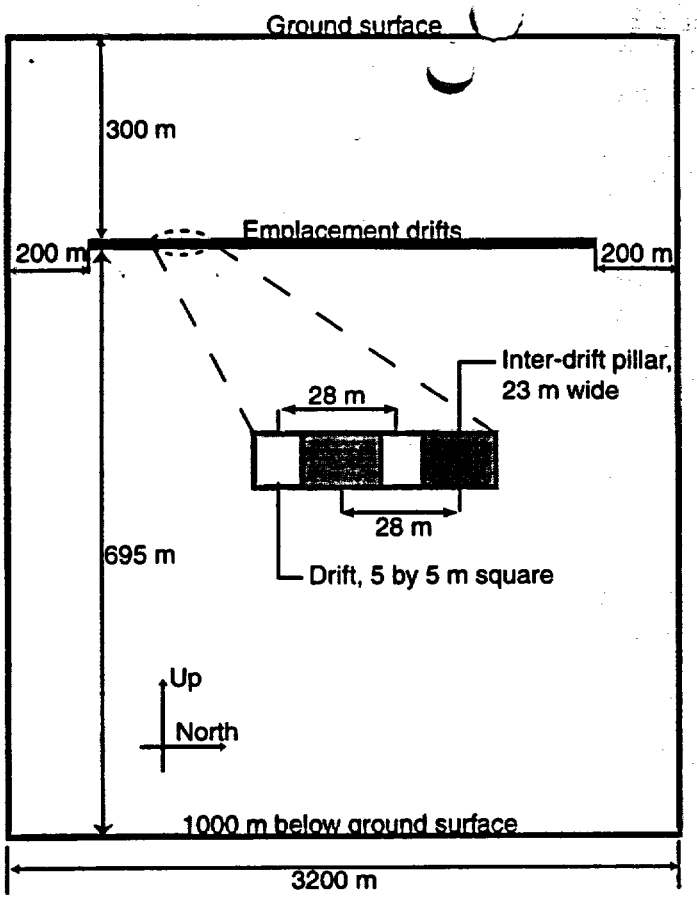

Figure 1. Schematic of model geometry

vertically, with the emplacement-drift axis at a depth of 302.5 m below the top.

Each emplacement drift was represented as a 5 × 5-m square opening. Precast concrete lining (the currently proposed support system for emplacement drifts) was represented in the model using beam elements superimposed on the edges of drift openings. The beam elements were assigned high stiffness to simulate the action of concrete-lining support and were removed at a stage in the model to simulate complete disintegration of the support. The currently proposed design calls for a circular cross section for the emplacement drifts. The use of a square section in this model is a simplification necessitated by the scale of the model. Appropriate circular sections would be used in a more detailed (such as drift-scale) model. The finite-element mesh consists of 4881 eight-noded quadrilateral elements that range in size from 5 × 5 m and 5 × 11.5 m near the openings to about 100 × 125 m near the base of the model. Possible effects of mesh density on the model results have not been investigated. Because stresses and material behavior were evaluated at element integration points, the theoretical stress concentration at the corners of the rectangular openings is not expected to have significant effects on the calculated response.

Boundary conditions consist of no boundary-normal displacement and no temperature change on the north, south, and base boundaries of the model. The top of the model (simulating the ground surface) was treated as a mechanically free surface with no temperature change. The perimeters of drift openings were also treated as mechanically free surfaces. Initial temperature was specified as a function of depth following the geothermal gradient for the site. Initial stress was specified using a depth gradient of 0.023 MPa/m for vertical stress and a horizontal to vertical stress ratio of 0.268 (cf. Stock et al. 1985). Thermal load was simulated as a time-decaying volumetric heat source applied uniformly within the perimeter of each emplacement drift.

2.1 *Material properties*

Mechanical properties that can be derived from the Q data were varied horizontally in the north-south direction of the model. Material properties were not varied vertically because of the lack of sufficient data to define vertical variation of properties in a manner consistent with the available Q data. Properties that cannot be derived from the Q data were assigned the values for the Topopah Spring Welded Unit 2 stratigraphic unit (Lin et al. 1993, Brechtel et al. 1995), as in Table 1.

Table 1. Material parameter values.

Parameter	Value
Density (kg/m^3)	2274
Thermal conductivity (W/m · K)	2.1
Specific heat (J/m^3 · K)	Temperature dependent, $(2.14 - 10.48) \times 10^{-6}$
Poisson's ratio, ν	0.21
Unconfined compressive strength of intact rock, σ_{ci} (MPa)	180
Thermal expansivity, α (K^{-1})	Temperature dependent, $(5.07 - 8.97) \times 10^{-6}$

The values of the rock-mass strength parameters (friction angle, ϕ, and cohesion, c) based on the Mohr-Coulomb failure criterion and Young's modulus, E, were estimated from Q using empirical relationships (Hoek 1994, Hoek & Brown 1997). Young's modulus was calculated using the equation (Serafim & Pereira 1983)

$$E = 10^{[(RMR - 10)/40]} \text{ GPa} \qquad (2.1)$$

where rock mass rating (RMR) is given by the equation (cf. Hoek 1994)

$$RMR = 9 \ln Q + 49 \quad (2.2)$$

Equation 2.1 provides a reasonable fit for the currently available empirical data describing the relationships between E and RMR or Q (Fig. 3 of Hoek 1994). Furthermore, because the Q values used in the model (0.7–13.6) lie within the range of the available empirical data, the values of E obtained using Equation 2.1 can be considered supported by empirical data. It is necessary, however, to obtain site-specific E-versus-RMR (or Q) data for the potential repository host rock mass to evaluate the applicability of Equation 2.1 (or similar equations) for the site. The values for ϕ and c were estimated from charts in Hoek & Brown (1997) using a value of 10 for the Hoek-Brown intact-rock parameter m_i (Brechtel et al. 1995) and values of geological strength index (GSI) given by (Hoek 1994)

$$GSI = 9 \ln Q + 44 \quad (2.3)$$

Analyses were also conducted using maximum possible ϕ values from the Hoek-Brown chart, corresponding to an m_i value of 35.

2.2 *Degradation of mechanical properties with time*

Rock-mass mechanical properties may degrade with time because of decrease in strength of intact rock under sustained long-term loading (Lajtai & Schmidtke 1986) and decrease in shear strength of fracture surfaces due to wall-rock alteration caused by extended exposure to heat and moisture.

It has been demonstrated through laboratory testing under sustained compressive loading (Lajtai & Schmidtke 1986) that the strength of intact hard rocks (e.g. granite, sandstone, or welded tuff) under slow or sustained loading may be much smaller than the strength obtained through conventional (usually rapid) laboratory loading conditions. The loading rate in sustained loading tests is slow enough to allow slow-growing fractures, such as may be driven by stress corrosion at crack tips, to extend and coalesce sufficiently to cause eventual rupture of the specimen. On the other hand, such fractures do not have sufficient time to grow under rapid loading conditions. For example, Lajtai & Schmidtke (1986) showed that long-term unconfined compressive strength of crystalline igneous rocks may be as low as 60 percent of their conventional unconfined compressive strength. Because the repository environment will be subjected to mechanical loading arising mainly from thermal expansion of rock under high temperatures that may be sustained for a long time (a few hundred years, at least), the strength of intact rock with the environment should be governed by b[illegible] under sustained loading. In the absence of any site-specific data, the long-term unconfined compressive strength of the intact rock was set to 50 percent of the conventional strength [i.e. σ_{ci} = 180 MPa for short-term (nondegraded) conditions and σ_{ci} = 90 MPa for long-term (degraded) conditions].

The long-term exposure of rock-fracture surfaces to moisture under elevated temperatures may create favorable conditions for chemical weathering of the fracture wall. The primary environmental factor necessary to trigger chemical weathering is the presence of an aqueous phase containing dissolved carbon dioxide (Nahon 1991), whereas the rate depends on the amount and temporal variation of water flux and temperature (Grim 1968, Nahon 1991). For example, chemical weathering is most rapid in warm, humid climates and least under dry conditions (Grim 1968). Although the climatic conditions at Yucca Mountain may imply that widespread chemical weathering of the rock mass is not likely, alteration of fracture-wall rocks at and near the repository depth should be of concern because of possible exposure of such fractures to moisture under elevated temperatures for periods of at least hundreds (and possibly thousands) of years. Such alteration of fracture-wall rock would result in fracture apertures widening in some areas and filling in other areas with material (such as clay) that is much weaker than the surrounding rock.

Such changes in fracture characteristics could weaken the rock mass, and the degree of weakening may be quantified through the rock-mass quality index, Q. Values of Q are calculated using six categorical variables that are assigned values to represent various aspects of the rock-mass condition following definitions provided by Barton et al. (1974). The values assigned to the various categories indicate that a change in fracture characteristics from "rough, irregular, and tightly healed" to "wide and filled with clay minerals thick enough to prevent wall-rock contact" would result in about one-order-of-magnitude decrease in the value of Q. Such a change would correspond approximately to fracture-surface conditions changing from "good" to "poor" in Hoek & Brown (1997). Therefore, Q values were reduced to 10 percent of their current values to represent the effects of fracture-wall rock alteration on rock-mass quality. This reduction of Q and the 50 percent reduction of σ_{ci} amount to a reduction of E, c, and ϕ from E = 8–36 GPa, c = 6.4–11.9 MPa, and ϕ = 28.4–35.4° for the current conditions to E = 2–11 GPa, c = 1.7–3.5 MPa, and ϕ = 22.7–30.2° for the mechanically degraded rock mass.

Time-dependent degradation of the mechanical properties of the ground-support material (e.g.

concrete) is also expected because of possible extended exposure of the materials to heat and moisture. In the currently proposed repository design, it is assumed that the ground-support system will degrade and eventually collapse following permanent closure of the proposed repository (U.S. Department of Energy 1998). Fractional degradation of the ground support was not represented in the current model. Instead, analyses were conducted to consider a fully effective ground-support system represented by the beam elements described earlier. Also, complete degradation of the support system was simulated by removing the beam elements at a stage of the analyses.

2.3 *Analysis cases*

Estimates of the rate of chemical weathering at the ground surface vary from about 0.5 to about 5 mm per 100 yr (Nahon 1991). Currently there is little information on rates of subsurface wall-rock alteration, but the information on surface weathering suggests it may take several tens (and maybe hundreds) of years for wall-rock alteration to become extensive enough to affect rock-mass quality. As a result, the sequence of thermal-mechanical response at the repository would consist of an initial period of stress buildup in an essentially nondegraded rock mass (mechanical behavior governed by current values of parameters) and a later period of increased effects of rock-mass degradation on mechanical behavior.

Because the magnitudes of thermal stress are controlled by the deformability parameters E, α, and ν, these parameters were assigned their current (i.e. nondegraded) values to model stress buildup correctly. On the other hand, the strength parameters ϕ, c, and σ_{ci}, were assigned their current values in an analysis case to examine the response of the

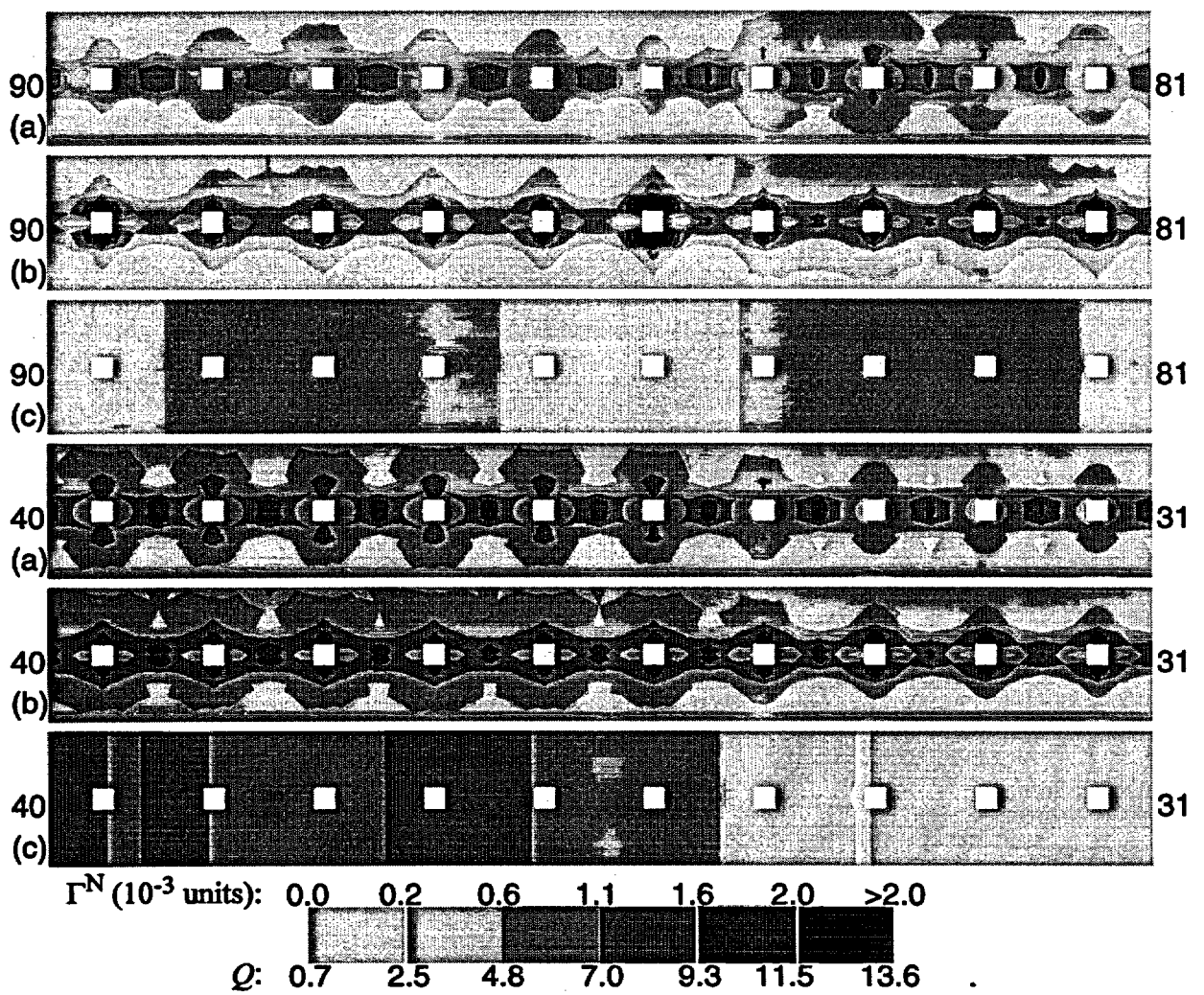

Figure 2. Distributions of inelastic-strain magnitude (equivalent plastic strain), Γ^N, and rock-mass quality index, Q, within a strip that extends vertically 17.5 m above and below the emplacement-drift axis and horizontally over 10 emplacement drifts (defined by the numbers shown at the ends of each section) for the case of degraded rock mass. Plots are (a) Γ^N for stiff-lining case, (b) Γ^N for degraded-lining case, and (c) Q.

an analysis case to examine the response of the nondegraded rock mass and their long-term (i.e. degraded) values in another case to obtain the response of the degraded rock mass.

First, a heat-conduction analysis was performed, using the boundary and initial conditions and thermal loading described earlier for a period of 150 yr from (instantaneous) waste emplacement. Thereafter, the resulting temperature histories were used as input for the two mechanical-analysis cases. For each case, the beam elements, which represent concrete lining, were left in place (with no degradation) during the entire 150 yr and were thereafter removed rapidly (with no temperature change) to simulate complete degradation of the liners. Hence, each mechanical-analysis case provides information to enable comparison of the states of ground movement with and without the lining. The simulation time of 150 yr is not significant by itself. The state of mechanical degradation simulated may develop during the preclosure period or a long time thereafter, depending on the rate of fracture-wall rock alteration. The representation of rock-mass degradation applied in the current model does not account for possible decrease in thermal stress (from cooling down) that might precede significant mechanical degradation of the rock mass. A time-dependent description of the entire phenomena may be required to better examine their effects on mechanical stability.

Excavation-induced deformations that would occur prior to the installation of drift support were not accounted for in the model. Preliminary analyses, however, show that the excavation-induced deformations are much smaller than the thermally induced deformations.

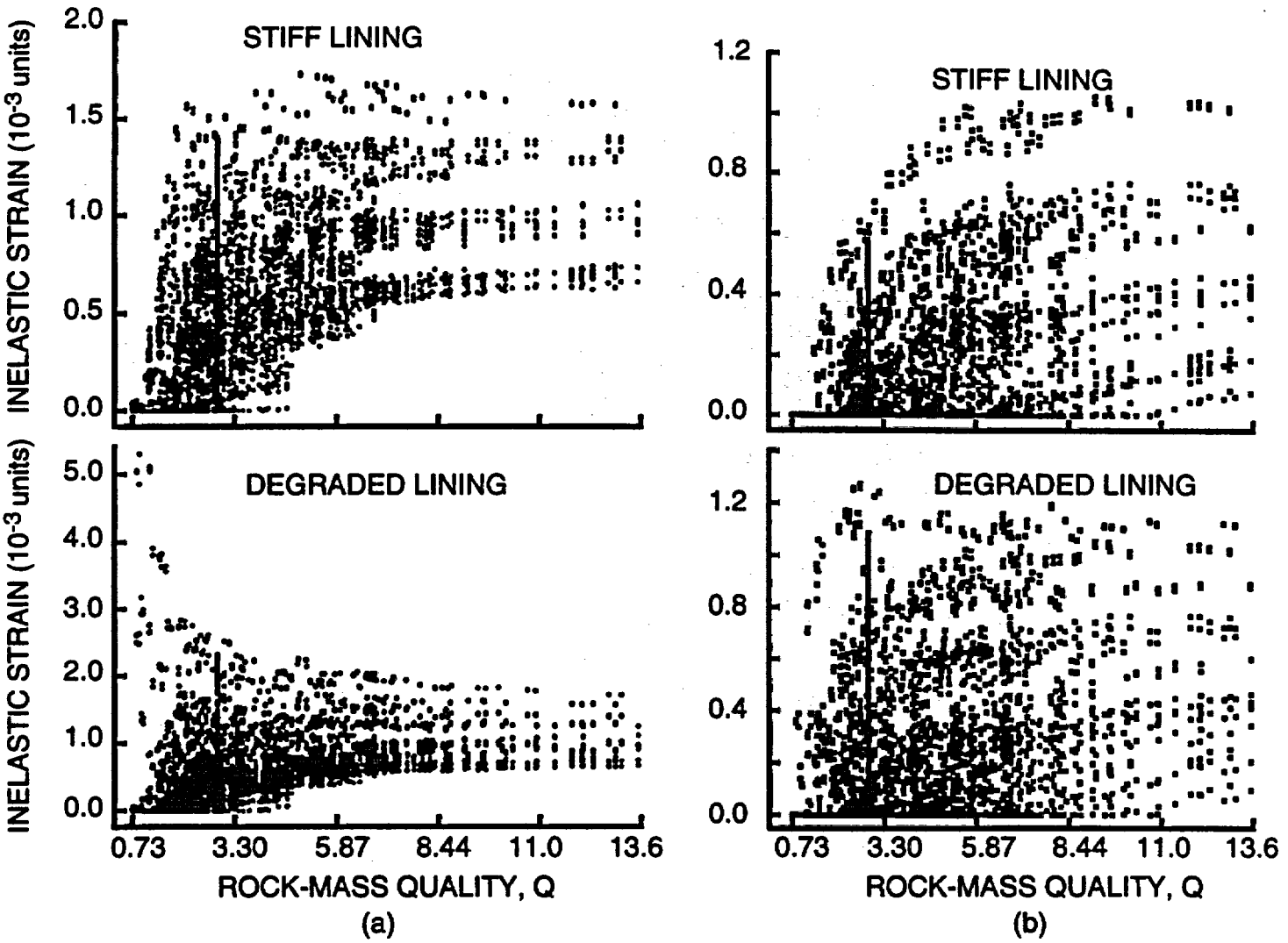

Figure 3. Magnitudes of inelastic strain (equivalent plastic strain) as functions of rock-mass quality index, Q, at element integration points within a strip that extends vertically 17.5 m above and below the emplacement-drift axis and horizontally across the entire model for the case of degraded rock mass: rock-mass friction angles were obtained from Hoek & Brown (1997) with (a) $m_i = 10$ and (b) $m_i = 35$.

3 RESULTS

The analysis results (Figs 2-3) are presented as distributions of the magnitude of inelastic strain Γ^N, also referred to as equivalent plastic strain (Ofoegbu & Curran 1992, Hibbitt, Karlsson & Sorensen, Inc. 1996). Inelastic strain in rocks is a manifestation of processes such as fracture growth, reopening and closing of existing fractures, and sliding on fracture surfaces. These processes, occurring individually or in combination, tend to cause loosening of the rock mass and, ultimately, the detachment of individual blocks. For this reason, it is expected that distributions of Γ^N may be interpreted, at least qualitatively, to indicate the distributions of potential instability. Results are presented for the cases of degraded rock mass only, because Γ^N values are small everywhere for the cases of nondegraded rock mass. The results for the cases of degraded rock mass lead to the following observations.

3.1 *Supported openings in degraded rock mass*

In the presence of stiff drift support, Γ^N attains maximum values at the middle of inter-drift pillarswith secondary maxima in the roof and floor areas of the openings. Generally, both the magnitude of Γ^N and the extent of potentially unstable zones (indicated by the occurrence of nonzero Γ^N) are higher in areas of higher Q. This Γ^N distribution pattern is illustrated in Figure 2 in which plots for Drifts 81–90 and 31–40 (stiff-lining case) show maximum Γ^N values in the pillar centers and secondary maxima over the roofs and under the floors of the openings. The distribution of Q values in the areas of the two sets of drifts is also shown in Figure 2. Comparison of the Q and Γ^N distributions illustrate the occurrence of higher Γ^N values and increased extent of potentially unstable zones in areas of higher Q for the stiff-lining case. The same trend of Γ^N increasing generally as Q increases is illustrated in Figure 3a (stiff-lining case). As the figure shows, every calculation point with a Q value of about 4.6 or more experienced inelastic straining in the stiff-lining case whereas several points with lower Q values did not.

The occurrence of higher values of Γ^N in areas of higher Q is caused by the higher values of rock-mass stiffness in such areas. Although both the stiffness and strength parameters increase with Q, E is more sensitive to changes in Q than is either ϕ or c, considering the values of these parameters calculated from the empirical relationships described earlier. As a result, the rock-strength difference between two points that have different Q values is smaller than the induced-stress difference. Consequently, the failure criterion is more likely satisfied in areas of higher Q (because of higher thermally induced stress) than in areas of lower Q. The relationship between Γ^N and Q is expected to be reversed (Γ^N decreasing as Q increases) at high Q values, probably much higher than the range of Q (0.7–13.6) used in the model. For such a reversal to occur, the empirical equations that relate values of Q (or any other rock-mass quality index) to mechanical parameters should result in strength-parameter values that increase faster than the stiffness-parameter values within such rock-mass quality range. The E-versus-Q relationship applied in the model, which is reasonably supported by the available empirical data (Fig. 3 of Hoek 1994), resulted in values of Γ^N that increase with Q even with the maximum possible values of friction angle from the empirical relationships. As shown in Figure 3b, an analysis case performed using the maximum friction angle curve (corresponding to m_i of 35) from Hoek & Brown (1997) shows Γ^N increasing generally as Q increases, for the stiff-lining case. Site-specific data defining the relationships between rock-mass quality and mechanical parameters for the proposed repository site would facilitate further investigations to determine the validity of the calculated relationship between Γ^N and Q (and its implications for the distribution of potential instability).

3.2 *Unsupported openings in degraded rock mass*

Degradation of drift support causes increased Γ^N everywhere, especially in the roof and floor areas of the drifts. Areas with lower Q values experience larger increases in Γ^N than corresponding areas with higher Q values. For example, Figure 3a shows several points with a Q value of about 0.73 that experienced essentially zero Γ^N in the stiff-lining case but up to 5 microstrain in the degraded-lining case. Also, as shown in Figure 2, values of Γ^N increased remarkably in the roof and floor areas of Drift #85 (located in an area of relatively low Q, as the figure shows) between the stiff-lining and degraded-lining cases. The figure illustrates general increase of Γ^N in the roof and floor areas owing to lining degradation, with greater increase in areas of lower Q. Since there was no change in temperature during the lining-removal analysis step, the difference between the stiff-lining and degraded-lining cases is caused by the stress change introduced by the removal of the lining. Such stress change resulted in loss of confinement and consequent increased inelastic straining in the roof and floor areas of the openings. The loss of confinement produced more severe effects in areas of lower Q than in areas of higher Q, resulting in a reversal of the Γ^N-versus-Q relationships as illustrated in Figure 3.

4 CONCLUSIONS

Both the intensity of potential instability and the extent of potentially unstable areas would vary spatially and

Ofoegbu 6

increase with time in the emplacement-drift area of the proposed repository because spatial variation and plausible time-dependent degradation of rock-mass mechanical properties. The mechanical parameters used in the analyses, however, were derived from rock-mass quality data using empirical relationships developed from measurements at other sites. The applicability of such empirical relationships at the proposed repository site needs to be evaluated through site-specific data defining the relationships between rock-mass mechanical properties and quality indices, such as Q or RMR.

ACKNOWLEDGMENT

This paper was prepared to document work performed by the Center for Nuclear Waste Regulatory Analyses (CNWRA) for the Nuclear Regulatory Commission (NRC) under Contract No. NRC-02-97-009. The activities reported here were performed on behalf of the NRC Office of Nuclear Material Safety and Safeguards, Division of Waste Management. This paper is an independent product of the CNWRA and does not necessarily reflect the view or regulatory position of the NRC.

REFERENCES

Barton, N., R. Lien, & J. Lunde. 1974. Engineering classification of rock masses for the design of tunnel support. *Rock Mechanics* 6: 189–236.

Bieniawski, Z.T. 1979. The geomechanics classification in rock engineering applications. In *Proceedings of the 4th International Congress on Rock Mechanics. Montreaux, Switzerland.* Rotterdam: A.A. Balkema Publishers 2: 41–48.

Brechtel, C.E., M. Lin, E. Martin, & D.S. Kessel. 1995. *Geotechnical Characterization of the North Ramp of the Exploratory Studies Facility. Vol. 1—Data Summary.* SAND95-0488/1. Albuquerque, NM: Sandia National Laboratories.

Civilian Radioactive Waste Management System, Management and Operating Contractor. 1997. *Confirmation of Empirical Design Methodologies.* BABEE0000-01717-5705-0000-2. Rev. 00. Las Vegas, NV: Office of Civilian Radioactive Waste Management.

Grim, R.E. 1968. *Clay Mineralogy.* New York: McGraw-Hill.

Hibbitt, Karlsson, & Sorensen, Inc. 1996. *ABAQUS User's Manual: Version 5.6.* Pawtucket, RI: Hibbitt, Karlsson, & Sorensen, Inc.

Hoek, E. 1994. Strength of rock and rock masses. *ISRM News Journal* 2(2): 4–16.

Hoek, E. & E.T. Brown. 1997. Practical estimates of rock mass strength. *Int. J. Rock Mech. and Mining Sci.* 34(8): 1165–1186.

Lajtai, E.Z. & R.H. Schmidtke. 1986. Delayed failure in rock loaded in axial compression. *Rock Mech. and Rock Eng.* 19: 11–25.

Lin, M., M.P. Hardy, J.F.T. Agapito & Associates & S.J. Bauer. 1993. *Rock Mass Mechanical Property Estimations for the Yucca Mountain Site Characterization Project.* SAND92-0450. Albuquerque, NM: Sandia National Laboratories.

Nahon, D.B. 1991. *Introduction to The Petrology of Soils and Chemical Weathering.* New York: John Wiley and Sons, Inc.

Ofoegbu, G.I. & J.H. Curran. 1992. Deformability of intact rock. *Int. J. Rock Mech. and Mining Sci.* 29(1): 35–48.

Serafim, J.L. & J.P. Pereira. 1983. Consideration of the geomechanical classification of Bieniawski. In *Proc. Int. Symp. on Engineering Geology and Underground Construction. Lisbon* 1(II): 33–44.

Stock, J.M., J.H. Healy, S.H. Hickman, & M.D. Zoback. 1985. Hydraulic fracturing stress measurements at Yucca Mountain, Nevada and relationship to regional stress field. *J. of Geophysical Res.* 90(B10): 8691–8706.

U.S. Department of Energy. 1998. *Viability Assessment of a Repository at Yucca Mountain, Volume 1: Introduction and Site Characteristics.* DOE/RW-0508/V1. Washington, DC: U.S. Department of Energy.